AGU PUBLICATIONS

JGR

Journal of Geophysical Research: Space Physics

RESEARCH ARTICLE
10.1002/2016JA022530

Key Points:
- Identify and measure plasma parameters local to the 3-D reconnection line in global MHD simulations with oblique IMF and dipole tilt
- Calculate 2-D analytic asymmetric reconnection rates from upstream plasma parameters
- Find the measured reconnection rate local to the 3-D reconnection line scales well with 2-D analytic predictions for all simulations

Correspondence to:
C. M. Komar,
colin.m.komar@gmail.com

Citation:
Komar, C. M., and P. A Cassak (2016), The local dayside reconnection rate for oblique interplanetary magnetic fields, *J. Geophys. Res. Space Physics*, *121*, 5105–5120, doi:10.1002/2016JA022530.

Received 12 FEB 2016
Accepted 5 MAY 2016
Accepted article online 13 MAY 2016
Published online 2 JUN 2016

The local dayside reconnection rate for oblique interplanetary magnetic fields

C. M. Komar[1,2,3] and P. A. Cassak[1]

[1]Department of Physics and Astronomy, West Virginia University, Morgantown, West Virginia, USA, [2]Geospace Physics Laboratory, NASA Goddard Space Flight Center, Greenbelt, Maryland, USA, [3]Department of Physics, Catholic University of America, Washington, District of Columbia, USA

Abstract We present an analysis of local properties of magnetic reconnection at the dayside magnetopause for various interplanetary magnetic field (IMF) orientations in global magnetospheric simulations. This has heretofore not been practical because it is difficult to locate where reconnection occurs for oblique IMF, but new techniques make this possible. The approach is to identify magnetic separators, the curves separating four regions of differing magnetic topology, which map the reconnection X line. The electric field parallel to the X line is the local reconnection rate. We compare results to a simple model of local two-dimensional asymmetric reconnection. To do so, we find the plasma parameters that locally drive reconnection in the magnetosheath and magnetosphere in planes perpendicular to the X line at a large number of points along the X line. The global magnetohydrodynamic simulations are from the three-dimensional Block-Adaptive, Tree Solarwind Roe-type Upwind Scheme (BATS-R-US) code with a uniform resistivity, although the techniques described here are extensible to any global magnetospheric simulation model. We find that the predicted local reconnection rates scale well with the measured values for all simulations, being nearly exact for due southward IMF. However, the absolute predictions differ by an undetermined constant of proportionality, whose magnitude increases as the IMF clock angle changes from southward to northward. We also show similar scaling agreement in a simulation with oblique southward IMF and a dipole tilt. The present results will be an important component of a full understanding of the local and global properties of dayside reconnection.

1. Introduction

Magnetic reconnection occurs where oppositely directed magnetic field components undergo a change of topology and subsequently combine together, resulting in energization of the plasma threaded by the magnetic field. The simple model of *Dungey* [1961, 1963] depicts reconnection occurring at the subsolar magnetopause under due southward interplanetary magnetic field (IMF) and no dipole tilt; when the IMF has the opposite orientation, reconnection occurs poleward of the magnetospheric cusps. Dayside reconnection couples solar wind plasma to the geomagnetic field and subsequently drives many processes observed in Earth's magnetosphere: magnetospheric convection [*Dungey*, 1961], expansion of the polar cap [see *Boudouridis et al.*, 2005, and references therein], and the development of plasmaspheric drainage plumes [see *Sandel et al.*, 2003, and references therein] among many others.

Recently, there has been increased debate regarding what physical parameters determine the rate at which reconnection proceeds at the dayside magnetopause, both globally and locally. As the solar wind is the primary driver of magnetospheric reconnection, it has been argued that the dayside reconnection site adjusts to reconnect the magnetic flux from the solar wind at the global rate it is injected [*Axford*, 1984]. This is quantified by coupling functions of the solar wind's geoeffectiveness. *Newell et al.* [2007] reviewed several models that have been used; all the ones listed only depend on solar wind plasma parameters, underscoring the long-held belief that geoeffectiveness is controlled by the solar wind. More recently, a theoretical model mapping the solar wind (convective) electric field to that of the subsolar magnetopause, i.e., the subsolar reconnection rate, was developed (J. C. Dorelli, private communication, 2015).

Recent arguments, however, suggest that this approach neglects contributions from the magnetospheric plasma that can affect the reconnection. *Borovsky and Denton* [2006] showed that geomagnetic indices decrease during times when plasmaspheric drainage plumes propagate to the dayside magnetopause.

It was argued that the plumes mass load the reconnection site resulting in slower Alfvén speeds, thus slowing reconnection. This "plasmasphere effect" has been further supported with total electron content observations [*Walsh et al.*, 2014a] and numerical simulations [*Borovsky et al.*, 2008; *Ouellette et al.*, 2016]. It has subsequently been argued that the plasmasphere effect changes the *local* reconnection rate, and concomitantly some geomagnetic indices, but does not change the *global* reconnection rate [*Lopez*, 2016]. However, mass loading the magnetosphere also decreases the global reconnected flux [*Zhang et al.*, 2016], and it was argued that plumes can change the global reconnection rate [*Ouellette et al.*, 2016]. Thus, what sets the local, and even the global, dayside reconnection rate remains an important and debated question.

In order to make definitive studies about these questions, one needs an approach to systematically locate and analyze the local properties of dayside reconnection. As we discuss below, there have been such numerical and observational studies in the past, but they have focused on cases with essentially due southward IMF, and the simulations have left out the dipole tilt. This study outlines an approach to this problem for the more generic and challenging case when the IMF is neither due southward nor due northward but rather makes an oblique angle relative to the geomagnetic field.

One model of local dayside reconnection that has been tested in the last decade is based on a scaling calculation of reconnection in asymmetric systems [*Cassak and Shay*, 2007]. The calculation has been tested in scaling studies of antiparallel asymmetric reconnection in two-dimensional (2-D) slab geometries in resistive magnetohydrodynamic (MHD) [*Borovsky and Hesse*, 2007; *Cassak and Shay*, 2007], two-fluid Hall MHD [*Cassak and Shay*, 2008, 2009], and particle-in-cell [*Malakit et al.*, 2010] simulations, and the predictions perform well. It is also successful in describing reconnection in 2-D resistive-MHD turbulence [*Servidio et al.*, 2009]. However, the original calculation was only for 2-D systems and did not include the effect of an out-of-plane magnetic field among other assumptions, so it is not a priori obvious that such a theory applies to the real 3-D dayside magnetopause.

Attempts have been made to determine its applicability to the 3-D magnetopause in global MHD simulations with due southward IMF and no dipole tilt [*Borovsky et al.*, 2008; *Ouellette et al.*, 2014]. In general, the reconnection rates measured in the simulations found agreement with the scaling relations presented in *Cassak and Shay* [2007]. When there was a plasmaspheric plume, the local reconnection rate decreased as predicted [*Borovsky et al.*, 2008]. We are not aware of any simulation studies addressing this topic at the dayside magnetopause for oblique IMF, and this remains beyond the scope of the present study.

Observationally, there have been tests of the theory. It was found to be successful in laboratory experiments [*Yoo et al.*, 2014; *Rosenberg et al.*, 2015] and may explain features of asymmetric X-ray emission from the foot points of solar flares [*Murphy et al.*, 2012]. In the magnetosphere, Polar observations of reconnection at Earth's dayside magnetopause have confirmed the scaling of the theory [*Mozer and Hull*, 2010]; the events studied were exclusively for nearly due southward IMF. It was shown observationally that reconnection slows locally when a plume reaches the dayside reconnection site [*Walsh et al.*, 2014a, 2014b]. Predictions of the substructure of the diffusion region have been observed [*Graham et al.*, 2014; *Muzamil et al.*, 2014]. The Cluster satellites were used to compare the theory with multiple events, showing a correlation between the predictions and the data [*Wang et al.*, 2015] (though see the paper for further discussion).

Assessing the applicability of asymmetric reconnection theory at the dayside magnetopause for oblique IMF orientations has been challenging since the precise locations on the magnetopause where reconnection occurs for such situations is not well understood. Several models to locate reconnection and its orientation exist [see, e.g., *Trattner et al.*, 2007; *Swisdak and Drake*, 2007; *Hesse et al.*, 2013], but a recent study found that none of the competing models are perfect for oblique IMF conditions [*Komar et al.*, 2015]. Knowing exactly where reconnection occurs is crucial for the questions being addressed here. An alternate approach is to determine the topology of the magnetic field and identify precisely the location of dayside reconnection as regions where different magnetic topologies converge. The curve that separates the four topologies (solar wind, terrestrial, and open to the solar wind on one end and piercing Earth's north or south pole on the other) is the magnetic separator, which marks the location where reconnection can occur. The reconnection X line, therefore, lies along the separator. While formally there are differences between separators and X lines because reconnection need not be happening everywhere along a separator, we tend to see in the magnetospheric geometry that reconnection does happen along most of the separator, so for the purposes of this paper we often use the words interchangeably. There now exist numerous methods to determine magnetic separators in global magnetospheric observations [*Xiao et al.*, 2007; *Pu et al.*, 2013] and simulations

[*Laitinen et al.*, 2006; *Hu et al.*, 2007; *Komar et al.*, 2013; *Stevenson and Parnell*, 2015; *Glocer et al.*, 2016], as well as in the solar context [*Longcope*, 1996; *Close et al.*, 2004; *Beveridge*, 2006]. This approach to finding reconnection sites has become practical and therefore is the approach used in this study.

In order to systematically study the applicability of asymmetric reconnection theory to the dayside magnetopause with obliquely oriented IMF and dipole tilt, one must carefully analyze the reconnection physics local to the X line. We adopt an approach similar to that of *Parnell et al.* [2010] for the solar context. Having previously located magnetic separators in our global magnetospheric resistive-MHD simulations with obliquely oriented IMF [*Komar et al.*, 2013] and nonzero dipole tilt [*Komar et al.*, 2015], we quantify local properties of reconnection on dayside portions of the X lines for multiple simulations. We go beyond previous work by systematically measuring local parameters in planes normal to the magnetic separator and comparing the measured reconnection rate at the separator to the predictions of local asymmetric reconnection theory. We find that the 2-D model reproduces the measured local electric fields along the X line quite well in the scaling sense, especially for the previously studied due southward IMF case where the agreement is nearly perfect. However, for oblique IMF, there is an absolute constant of proportionality not captured by the model which becomes more significant as the IMF clock angle decreases from 180°. The results are similar for systems with a dipole tilt. We also show that care must be employed to ensure proper resolution of the diffusion region for studies of this sort.

The layout of this paper is as follows: Section 2 provides a brief overview of the 2-D asymmetric reconnection scaling relations that are tested in the present study, describes our simulation setup, summarizes the method employed to determine the magnetic separators in our global simulations, and outlines the systematic approach used to measure the local plasma parameters that are used to calculate the local asymmetric reconnection rate from the scaling relations. Our simulation results are presented in section 3. Finally, a brief summary of our results and their applications are discussed in section 4.

2. Methodology

2.1. Reconnection Model to Compare With Simulations

The analytical model we compare to our simulations assumes upstream conditions with a magnetospheric plasma of density ρ_{MS} and reconnecting magnetic field component of strength B_{MS} with magnetosheath plasma having density ρ_{SH} and reconnecting magnetic field strength B_{SH}. The asymmetric reconnection rate E_{asym} scales as [*Cassak and Shay*, 2007]

$$E_{\mathrm{asym}} \sim \frac{B_{\mathrm{MS}}B_{\mathrm{SH}}}{B_{\mathrm{MS}}+B_{\mathrm{SH}}} c_{A,\mathrm{asym}} \frac{2\delta}{L}, \tag{1}$$

where

$$c_{A,\mathrm{asym}}^2 \sim \frac{B_{\mathrm{MS}}B_{\mathrm{SH}}}{\mu_0 \rho_{\mathrm{out}}} \tag{2}$$

is the predicted outflow speed, μ_0 is the permeability of free space, the predicted outflow density ρ_{out} is

$$\rho_{\mathrm{out}} \sim \frac{\rho_{\mathrm{MS}}B_{\mathrm{SH}}+\rho_{\mathrm{SH}}B_{\mathrm{MS}}}{B_{\mathrm{MS}}+B_{\mathrm{SH}}}, \tag{3}$$

and δ and L are the half-width and half-length of the dissipation region, respectively. This prediction makes no assumption about the dissipation mechanism.

For the special case of resistive reconnection, as is the case for the simulations in the present study, the reconnection rate $E_{\eta,\mathrm{asym}}$ was shown to scale as [*Cassak and Shay*, 2007]

$$E_{\eta,\mathrm{asym}} \sim \sqrt{\frac{\eta c_{A,\mathrm{asym}}}{\mu_0 L} B_{\mathrm{MS}}B_{\mathrm{SH}}}, \tag{4}$$

where η is the resistivity.

We will test equations (1) and (4) in our global magnetospheric simulations. However, it bears noting that there are limitations to the theory. It is typically assumed that the magnetic field component parallel to the X line, known as the guide field, does not affect the reconnection rate or dynamics of the dissipation region.

This is unlikely to be the case in the real system as finite Larmor radius effects have important consequences for reconnection [*Swisdak et al.*, 2003, 2010; *Beidler and Cassak*, 2011; *Malakit et al.*, 2013]. However, these effects are not present in the resistive-MHD model used for our global simulation study, so this assumption may be acceptable for the present study. Also, the theory does not include the effect of the solar wind flow on the magnetosheath side of the magnetopause, which may also be important [*Doss et al.*, 2015].

2.2. Global Magnetospheric Simulations

We perform global simulations using the Space Weather Modeling Framework (SWMF) [*Tóth et al.*, 2005, 2012], a suite of physical models developed at the University of Michigan used to model regions from the Sun to the magnetosphere and beyond, although the methods detailed here can be adapted to other global magnetospheric codes. We specifically employ the Block-Adaptive, Tree Solarwind Roe-type Upwind Scheme (BATS-R-US) MHD code to solve the resistive-MHD equations on a high-resolution, three-dimensional, rectangular, and irregular grid in order to simulate the global magnetosphere [*Powell et al.*, 1999; *Gombosi et al.*, 2000; *De Zeeuw et al.*, 2000]. The ionosphere is modeled with the ionospheric electrodynamics (IE) component.

The simulations are performed at NASA's Community Coordinated Modeling Center (CCMC), a freely available code repository administered by NASA Goddard Space Flight Center. The CCMC's Kameleon software suite, which was developed by the CCMC to analyze the standardized output of different simulation models performed at the CCMC, is used to partially analyze simulation output of BATS-R-US by sampling data and tracing magnetic field lines at arbitrary coordinates within the simulation domain. The simulation domain is $-255 < x < 33$, $-48 < y < 48$, and $-48 < z < 48$, where distances are measured in Earth radii (R_E) and the coordinate system is geocentric solar magnetic (GSM). The simulations are run using BATS-R-US version 8.01.

The simulations are evolved for 2 h (02:00:00) of magnetospheric time, and we look at the 02:00:00 mark of simulation data when the dayside magnetopause has achieved a quasi-steady state. This is determined by comparing the location of the current density J_y along the x axis at adjacent time outputs (every 00:10:00); we find the current layer along the x axis is approximately stationary after 01:30:00 of magnetospheric time. The standard high-resolution grid for CCMC simulations has 1,958,688 grid cells with a coarse resolution of 8 R_E in the far magnetotail and a fine resolution of 0.25 R_E near the magnetopause. The simulations presented here employ a maximum resolution of 0.125 R_E throughout the region $-15 < x, y, z < 15$ $\mathrm{R_E}$, totaling 16,286,400 grid cells.

The boundary condition at $x = 33$ $\mathrm{R_E}$ uses constant solar wind values, although BATS-R-US is capable of using event data measured by solar wind monitors. We use solar wind temperature $T_{\mathrm{SW}} = 232,100$ K (20 eV), IMF strength $B_{\mathrm{IMF}} = 20$ nT, number density $n_{\mathrm{SW}} = 20$ cm^{-3}, and a solar wind velocity of $\mathbf{v}_{\mathrm{SW}} = -400$ km/s $\hat{\mathbf{x}}$ unless otherwise noted. These values for n_{SW} and B_{IMF} are somewhat high, but this enables the high-resolution region at the dayside magnetopause to not be as large. We also have investigated simulations with lower B_{IMF}. We perform distinct simulations with IMF clock angles θ_{IMF}=30°, 60°, 90°, 120°, 150°, and 180° (southward). The IMF does not have a B_x component. For the present simulations, we additionally employ a uniform explicit resistivity $\eta/\mu_0 = 6.0 \times 10^{10}$ m^2/s. Although the magnetosphere is known to be collisionless, including an explicit resistivity allows for reproducible results that are independent of the numerics [*Komar et al.*, 2013].

The IE component of the SWMF uses the currents of the MHD simulation at 3.5 R_E to determine the ionospheric currents at a radial distance of 1.017 R_E using conservation of electric charge. Constant Pederson and Hall conductances of 5 mhos are used to determine the ionospheric electric field $\mathbf{E}$ from these ionospheric currents at geomagnetic latitude and longitude discretized into 1° increments resulting in a 181 × 181 spherical grid.

2.3. Identification of X Lines in Global Simulations

We employ the separator mapping algorithm of *Komar et al.* [2013] which has been shown to reliably trace the dayside portion of X lines in global magnetosphere simulations for any IMF orientation and dipole tilt [*Komar et al.*, 2015]. In the separator tracing algorithm, a hemisphere is initially centered around a magnetic null. The hemisphere's surface, of radius 1 R_E for our purposes, is discretized into a grid. The magnetic field lines piercing the hemisphere at each grid point are traced to determine their magnetic topology. The approximate location of the separator is determined by finding where four magnetic topologies meet on the hemisphere's surface. Then, another hemisphere is centered at the determined separator location, and the procedure is iterated to trace the separator. The dayside separator is traced from northern to southern null in this fashion. An example is shown in Figure 1a for the $\theta_{\mathrm{IMF}} = 90°$ simulation. Open field lines are gray, and the X line is red.

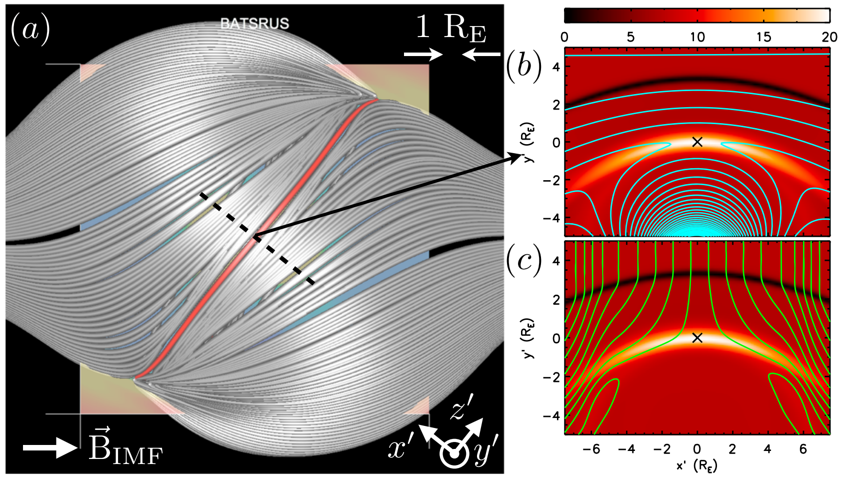

Figure 1. The plane normal to the X line at the subsolar magnetopause in a simulation with θ_{IMF}=90°. (a) The orientation of the plane centered at $\mathbf{r}_{\mathrm{Sep}} = (8.4,\ 0.0,\ 0.0)\ R_E$ in GSM coordinates (dashed black line). (b and c) The out-of-plane current density $J_{z'}$ in this plane as the color background in nA/m^2 and displays contours of (Figure 1b) the flux function Ψ in cyan and (Figure 1c) contours of the stream function Φ in green. The X line is located at (0, 0) in the x'-y' plane and marked with an X.

2.4. Determination of Planes Normal to the X Line

The separator tracing algorithm presented in *Komar et al.* [2013] results in a number (∼30) of locations lying along each X line. It is typically assumed that the plane of reconnection is normal to the X line. However, *Parnell et al.* [2010] analyzed reconnection local to separators in resistive-MHD simulations; they argued that the plane containing reconnection can often be the plane oriented normal to the separator but is not necessarily a general feature. For the purposes of this study, we adopt the assumption that the plane of reconnection is normal to the X line. This assumption fails as one approaches the nulls, so we caution the reader that this assumption needs further scrutiny.

We develop a procedure to construct planes normal to the X line by defining an orthonormal basis at every point along the X line. As a motivation for the procedure, consider the X line in Figure 1a. The plane normal to the X line at the subsolar point $\mathbf{r}_{\mathrm{Sep}} = (8.4,\ 0.0,\ 0.0)$ is sketched as the dashed line. We define a coordinate system $(x',\ y',\ z')$ for this plane. The out-of-plane unit vector $\hat{\mathbf{z}}'$ points along the X line, i.e., along the magnetic field with $\hat{\mathbf{z}}' = 0.62\hat{\mathbf{y}} + 0.78\hat{\mathbf{z}}$, with unprimed vectors given in GSM. We define the y' direction as the inflow direction and x' as the outflow direction. For the case study, the inflow direction at the subsolar point is radially out, so $\hat{\mathbf{y}}' = \hat{\mathbf{x}}$. Finally, the in-plane unit vector completing the orthonormal triplet is defined by $\hat{\mathbf{x}}' = \hat{\mathbf{y}}' \times \hat{\mathbf{z}}'$.

With this simple case in mind, we now describe the method by which we determine this coordinate system at arbitrary points on X lines. For the kth location along the X line, the out-of-plane unit vector $\hat{\mathbf{z}}'_k$ is tangent to the X line. Using a second order finite difference, this gives

$$\hat{\mathbf{z}}'_k = \frac{\mathbf{r}_{k-1} - \mathbf{r}_{k+1}}{\left|\mathbf{r}_{k-1} - \mathbf{r}_{k+1}\right|}, \tag{5}$$

where $\mathbf{r}_{k-1}$ and $\mathbf{r}_{k+1}$ are the previous and subsequent X line locations, respectively. We note that one could think of defining $\hat{\mathbf{z}}'_k$ by the magnetic field direction $\hat{\mathbf{b}}$ at the X line, but this definition fails when the magnetic field parallel to the separator is small, such as for due southward IMF (θ_{IMF}=180°). The formulation of equation (5) guarantees a meaningful $\hat{\mathbf{z}}'_k$ for *any* IMF orientation and magnetospheric dipole tilt.

The unit vector $\hat{\mathbf{y}}'_k$ in the direction of the inflow is given by the normal to the magnetopause at $\mathbf{r}_k$. This is calculated by finding the projection of $\mathbf{r}_k$ normal to $\hat{\mathbf{z}}'_k$. Mathematically, this is represented as

$$\hat{\mathbf{y}}'_k \propto \mathbf{r}_k - \left(\mathbf{r}_k \cdot \hat{\mathbf{z}}'_k\right) \hat{\mathbf{z}}'_k. \tag{6}$$

Finally, $\hat{\mathbf{x}}'_k$ completes the right-handed triplet by taking the cross product

$$\hat{\mathbf{x}}'_k = \hat{\mathbf{y}}'_k \times \hat{\mathbf{z}}'_k. \tag{7}$$

We note that the coordinate system resulting from this process is similar to the boundary normal (*LMN*) coordinate system. The three directions are analogous to their counterparts where $\hat{\mathbf{x}}' \equiv \hat{\mathbf{L}}$, pointing in the direction of the reconnecting component of the magnetic field and corresponding to the reconnection outflow direction, $\hat{\mathbf{y}}' \equiv \hat{\mathbf{N}}$ is the inflow direction, and $\hat{\mathbf{z}}' \equiv -\hat{\mathbf{M}}$ is the out-of-plane (guide field) direction. We do not employ minimum variance analysis [*Sonnerup and Cahill*, 1967], however, because it does not always give appropriate results, especially when there is a guide field.

With this orthonormal basis, the x'-y' plane is assumed to be the plane of reconnection. Coordinates of locations in this plane are translated back to GSM coordinates, and Kameleon is used to sample the plasma number density n, thermal pressure p, magnetic field $\mathbf{B}$, plasma flow $\mathbf{u}$, and current density $\mathbf{J}$ in this plane. Each plane spans $-7.5 \leq x' \leq 7.5$ and $-5 \leq y' \leq 5\,R_E$ and each direction is sampled in $\Delta x' = \Delta y' = 0.0625\,R_E$ increments; the X line is centered at (0, 0) in each x'-y' plane. Finally, the magnetic field $\mathbf{B}$, plasma flow $\mathbf{u}$, and current density $\mathbf{J}$ vectors are transformed from GSM coordinates to the primed planar coordinates at the X line, e.g., $B_{x'} = \mathbf{B} \cdot \hat{\mathbf{x}}'$.

We show the results of this procedure for the simulation with $\theta_{\rm IMF}$=90° in Figure 1. Figures 1b and 1c display the out-of-plane current density component $J_{z'}$ as the color background in nA/m^2. The X line's location in the x'-y' plane is marked with an X at (0, 0).

In order to gain insight into what reconnection might look like in this plane, we employ a method used in 2-D geometries based on the flux function to determine the structure of the magnetic field. It is not formally generalizable to 3-D, but this is carried out only for perspective, and no conclusions are drawn from the results. If we ignore any dependence in the z' direction, then we can define a flux function $\Psi(x', y')$ as

$$\mathbf{B} = -\hat{\mathbf{z}}' \times \nabla'\Psi, \tag{8}$$

where the magnetic field $\mathbf{B}$ and derivatives ∇' are only considered in the x'-y' plane. Lines of constant Ψ represent the projection of magnetic field lines into the plane. The projected magnetic field lines are depicted in cyan in Figure 1b. We similarly define a 2-D stream function Φ to obtain the streamlines (field lines of the velocity vector) in the x'-y' plane with the simple substitution of Φ for Ψ and bulk velocity $\mathbf{u}$ for $\mathbf{B}$ in equation (8). Figure 1c displays contours of constant Φ in green which give the in-plane streamlines.

Figure 1 displays several features that are qualitatively consistent with the local picture of 2-D Sweet-Parker collisional reconnection [*Parker*, 1957; *Sweet*, 1958] and is consistent with the field structures described in *Parnell et al.* [2010], albeit occurring at the dayside magnetopause with a dipolar magnetic field. First, the out-of-plane current layer is elongated. The reconnecting magnetic field components are oppositely directed with the IMF pointing along $-\hat{\mathbf{x}}'$ and is carried along $-\hat{\mathbf{y}}'$ in the magnetosheath; the terrestrial magnetic field points along $+\hat{\mathbf{x}}'$ and slowly convects toward the magnetopause along $+\hat{\mathbf{y}}'$. These magnetic fields undergo reconnection at the X line with newly reconnected magnetic flux located downstream of the X line and displaying a curved X point reconnection geometry. Lastly, the plasma convects horizontally outward from the X line along y' with speeds $|\mathbf{u}| \approx 205$ km/s, higher than the vertically directed magnetosheath flow speed $|\mathbf{u}| \approx 150$ km/s. This suggests reconnection has a role in accelerating the outflowing plasma. Thus, the plane normal to the X line *at the subsolar magnetopause* qualitatively resembles 2-D pictures of reconnection.

We note that using equation (8) to determine magnetic field lines and streamlines in planes normal to the reconnection line is only rigorously valid for 2-D systems, so it should not be expected to be valid for arbitrary conditions. It likely works remarkably well for the plane we show because of the high degree of symmetry at the subsolar magnetopause in this simulation. We point out, however, that none of the subsequent analysis is dependent on the fields determined in this way; it is merely being shown here to illustrate that the magnetic field and flow in planes normal to the reconnection line reasonably appear like those of 2-D reconnection models.

2.5. Measuring Plasma Parameters in Planes Normal to the X Line

To analyze the reconnection in each plane and compare to the theory in section 2.1, we need the plasma parameters just upstream of the dissipation region. We start by sampling the out-of-plane current density $J_{z'}$ along $\hat{\mathbf{y}}'$ at x'= 0 to determine the location of maximum current density $J_{\rm max}$. Note that $J_{\rm max}$ may not be located at the X line and can be offset during asymmetric reconnection at the dayside magnetopause [*Cassak and Shay*, 2007; *Komar et al.*, 2015]. We define the full width, half max of $J_{z'}$ as the dissipation region's thickness 2δ.

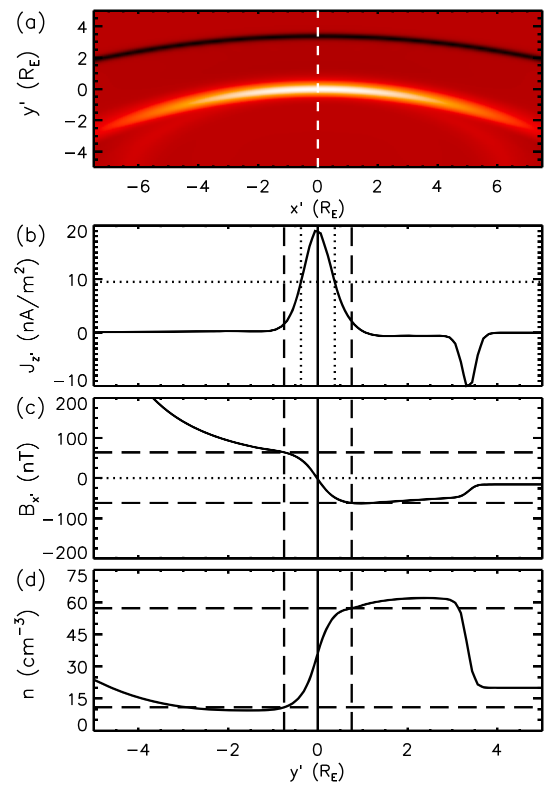

Figure 2. Determination of the upstream plasma parameters in the simulation with θ_{IMF}=90° for the plane at the subsolar point from Figure 1. (a) Out-of-plane current density $J_{z'}$; the white dashed line at $x' = 0$ displays the line along which plasma parameters are sampled. (b) $J_{z'}$ along $x' = 0$ with the X line's location depicted by the solid line. Locations where $J_{z'} = 0.5J_{max}$ are marked by vertical dotted lines. The value of $0.5J_{max}$ is marked by the horizontal dotted line. The vertical dashed lines in Figures 2b–2d indicate where magnetospheric and magnetosheath parameters are measured. (c) Reconnecting magnetic field component $B_{x'}$ in nT. (d) Plasma number density n in cm^{-3}. The horizontal lines in Figures 2c and 2d mark the magnetospheric and magnetosheath values of these parameters.

We define y'_{SH} and y'_{MS} as the locations corresponding to the magnetosheath and magnetospheric edges where the current is $0.5J_{max}$. The magnetosheath and magnetosphere pressures, densities, and the flow and magnetic field components are measured at $\left(0,\, y'_{SH} + \delta\right)$ and $\left(0,\, y'_{MS} - \delta\right)$, respectively, in the x'-y' plane.

An example of this procedure is demonstrated in Figure 2, which is the same plane displayed in Figure 1. Figure 1a displays the out-of-plane current density $J_{z'}$ as the color background with a dashed white line at $x' = 0$, the line along which the plasma parameters are sampled. Figure 1b shows the out-of-plane current density along $x' = 0$, with vertical dotted lines at the locations y'_{MS} and y'_{SH} where the current density has the value $0.5J_{max}$, marked with a horizontal dotted line. The X line's location is marked with a solid vertical line at $y' = 0$. The left and right dashed vertical lines mark $y'_{MS} - \delta$ and $y'_{SH} + \delta$ where the magnetospheric and magnetosheath plasma parameters are measured, respectively. Figure 1c displays the reconnecting magnetic field component $B_{x'}$ in nT, and Figure 1d displays the plasma number density n in cm^{-3}, respectively, along the same cut. The locations where the upstream parameters are sampled are again displayed with vertical dashed lines. Dashed horizontal lines in Figures 1c and 1d display the values obtained from this analysis. One can see that each determined parameter is representative of the asymptotic regions upstream of the dissipation region, as desired. The upstream values for this plane on the magnetospheric side are $B_{x',MS} = 64$ nT and $n_{MS} = 11$ cm^{-3}, and for the magnetosheath plasma are $B_{x',SH} = -61$ nT, and $n_{SH} = 57$ cm^{-3}; the dissipation region has half-width $\delta = 0.38\ R_E$.

In order to check the validity of the asymmetric reconnection scaling relations, we must also determine the half-length L of the dissipation region (see equations (1) and (4)). Care must be taken in determining the dissipation region length as it is curved due to the structure of Earth's magnetosphere. We therefore start by identifying the reconnection dissipation region by sampling the out-of-plane current density $J_{z'}$ along cuts oriented at an angle θ from the $+x'$ axis in the x'-y' plane as displayed in Figure 3a; the cuts start at $(0, -5)\ R_E$,

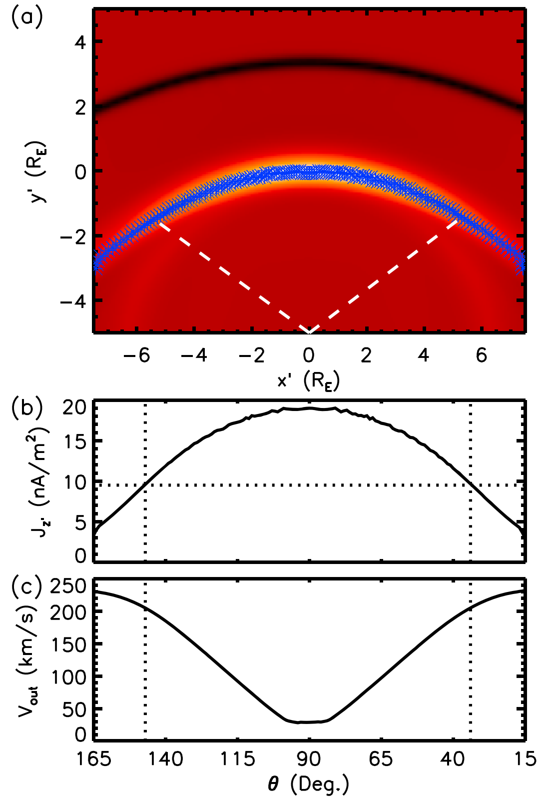

Figure 3. Determination of the dissipation region half-length L and outflow speed V_{out} for the plane in Figure 1. (a) Out-of-plane current density $J_{z'}$. The locations of current maxima are displayed as blue asterisks. (b) Current density maxima in nA/m^2 and (c) magnitude of V_{out} in km/s as functions of sampling angle θ measured from the $+x'$ axis. The left and right edges θ_{Left} and θ_{Right} of the dissipation region are displayed as dotted vertical lines in Figures 3b and 3c and are determined by where the current density maximum falls to $0.5J_{max}$, indicated by the horizontal dotted line in Figure 3b.

and the current density is sampled in 1/16 R_E increments, with θ discretized into 1° increments from [0°, 180°]. The location and value of the first current density maximum along each cut is retained. The right and left edges of the dissipation region are defined as θ_{Right} and θ_{Left} where the current density maximum first achieves a value of $J_{z'} = 0.5J_{max}$, where J_{max} is the aforementioned maximum current density value along $x' = 0$. L is directly calculated from the arc length of the measured current density maxima locations as

$$2L = \int_{\theta_{Right}}^{\theta_{Left}} dS \simeq \sum_{j=\theta_{Right}}^{\theta_{Left}} \Delta S_j, \tag{9}$$

where ΔS_j is the distance between the jth current density maximum at $\mathbf{S}_j$ and its neighbor at $\mathbf{S}_{j+1}$ is given by

$$\Delta S_j = \left|\mathbf{S}_{j+1} - \mathbf{S}_j\right|.$$

The outflow speed V_{out} is sampled separately along cuts in θ. The outflow speed maxima occur consistently on the magnetospheric side of the dissipation region, consistent with previous 2-D asymmetric reconnection simulations which measured the outflows on the side with higher Alfvén speed [*Cassak and Shay*, 2007; *Birn et al.*, 2008]. The left and right measured outflow velocities are both 205 km/s. We note that the outflow speeds in each direction are identical at the subsolar point, but they are not in planes away from the subsolar point. This asymmetric outflow could be related to differences in the outflow pressures which has been shown to affect the outflow speeds [*Murphy et al.*, 2010].

Figure 3 displays the results of this current density sampling method for the plane normal to the X line at the subsolar magnetopause in the θ_{IMF}=90° simulation. Figure 3a displays the current density maxima as

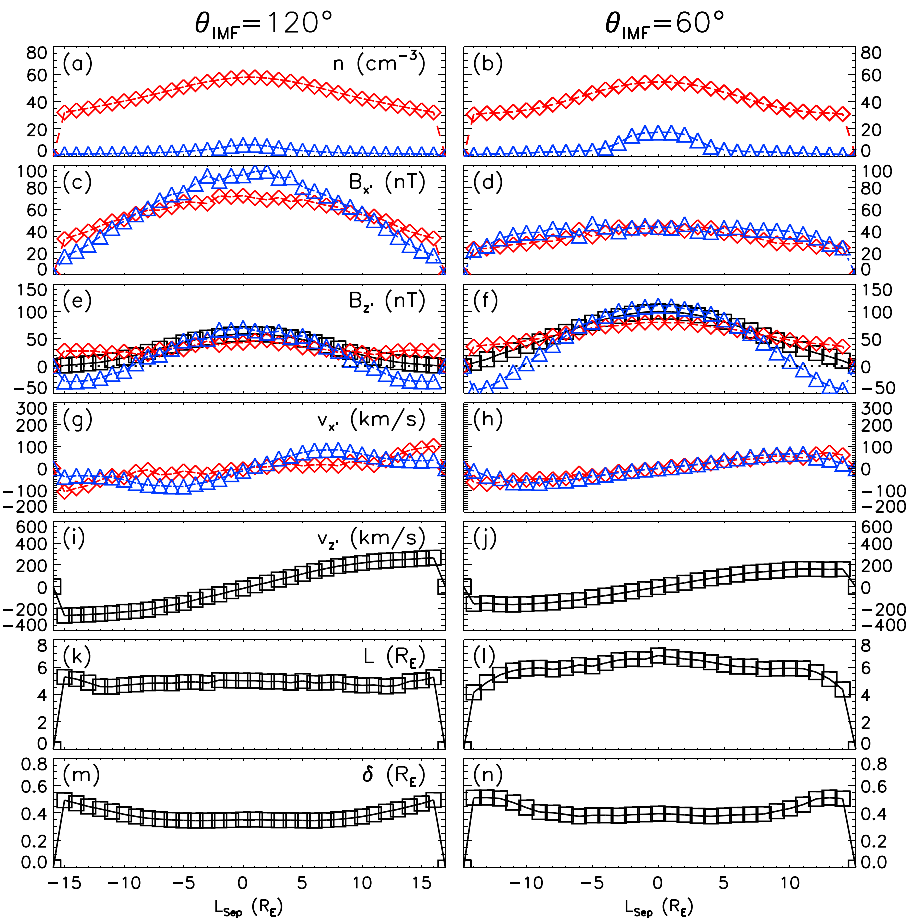

Figure 4. Plasma parameters at the magnetopause (black □), on the magnetospheric side (blue △), and on the magnetosheath side (red ◇) obtained with the techniques described in the text. (a, c, e, g, i, k, and m) θ_{IMF} = 120° and (b, d, f, h, j, l, and n) 60°, respectively. Displayed in each figure are the following: (Figures 4a and 4b) plasma number density n in cm^{-3}; (Figures 4c and 4d) reconnecting magnetic field component $B_{x'}$ in nT; (Figures 4e and 4f) out-of-plane (guide) magnetic field component $B_{z'}$ in nT; (Figures 4g and 4h) flow parallel to the reconnecting magnetic field component $u_{x'}$ in km/s; (Figures 4i and 4j) out-of-plane flow $u_{z'}$ in km/s; (Figures 4k and 4l) half-length L of the dissipation region in R_E; and (Figures 4m and 4n) half-width δ of the dissipation region. All parameters are displayed as functions of L_{Sep}, the duskward distance along the X line from the subsolar point.

blue asterisks. Figure 3b displays current density maxima values in nA/m^2, and Figure 3c displays the outflow velocity V_{out} in km/s as functions of the sampling angle θ. Vertical dotted lines display the determined locations of θ_{Left} and θ_{Right}, with the horizontal dotted line displaying $0.5J_{max}$. The dissipation region's half-length $L = 5.84\ R_E$ for this plane.

We have now measured all of the relevant parameters to make a meaningful comparison with the theoretical asymmetric reconnection scaling relations and the reconnection rate measured in our global simulations. We give two examples of the upstream parameters obtained from this approach in Figure 4, which show the sampled plasma parameters in our simulations with θ_{IMF}=120° (a, c, e, g, i, k, and m) and 60° (b, d, f, h, j, l, and n) as a function of L_{Sep}, the duskward distance along the separator relative to the subsolar magnetopause in R_E; positive values lie along the northern and dusk flank. From the upstream reconnecting magnetic field components $B_{x'}$ and densities n, the dissipation region's half-width δ and half-length L, we can calculate E_{asym} and $E_{\eta,asym}$ from the asymmetric scaling relations given by equations (1) and (4), respectively. Both of these are compared with the local reconnection rate at the X line $E_{z'} = \eta J_{z'}$. The procedure outlined here is repeated for all planes normal to the X line for all simulations in this study.

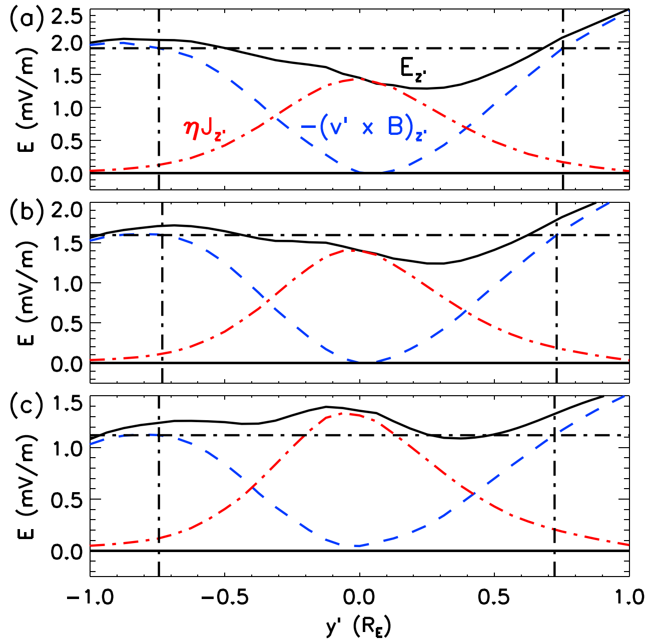

Figure 5. Contributions to Ohm's law in three representative planes for the simulation shown in Figure 1. The figures show the convective (blue dashed), resistive (red dash dotted), and total (black solid) out-of-plane electric field $E_{z'}$ in planes at L_{Sep} of (a) 0, (b) 5, and (c) 7 R_E duskward from the subsolar point.

3. Results

First, we show the contributions to Ohm's law in representative planes normal to the X line to motivate that the results presented here are reasonable. Figure 5 shows the convective (blue dashed), resistive (red dash dotted), and total (black solid) electric fields in the out-of-plane (z') direction. The panels are at L_{Sep} of (a) 0 (the subsolar point), (b) 5, and (c) 7 R_E for the simulation shown in Figure 1. In calculating the convective electric field, we boost into the reference frame making the upstream values equal, i.e., the reference frame of the X line, using a technique used previously [*Mozer et al.*, 2002; *Cassak and Shay*, 2009]. The vertical dash-dotted lines are the upstream positions, and the horizontal dash-dotted line is the electric field at those positions. The results reveal that the resistive electric field is nearly equal to the convective electric field in all three planes, which (1) confirms that the explicit resistivity is providing the dissipation (rather than numerical effects), (2) suggests that the steady state assumption is valid, and (3) suggests the approach we are using to find the plane of reconnection is reasonable.

Figure 6 displays the measured reconnection rate $E_{z'}$ (black squares) in mV/m along the separator in distinct simulations with θ_{IMF} of (a) 180°, (b) 150°, (c) 120°, (g) 90°, (h) 60°, and (i) 30°. Also displayed are the theoretical asymmetric reconnection rates E_{asym} (blue diamonds) and $E_{\eta,asym}$ (red triangles) given by equations (1) and (4), respectively. The reconnection rates are plotted as a function of L_{Sep}. Note that the vertical scale is different for different θ_{IMF}; reconnection is faster for southward IMF than northward IMF, as is well known.

The comparison between theoretical and measured values for θ_{IMF} = 180° in Figure 6a reveals that the prediction is exceedingly good; they are almost indistinguishable. This is consistent with previous results of *Borovsky et al.* [2008] and *Ouellette et al.* [2014]. The other clock angle simulations in Figures 6b, 6c, and 6g–6i reveal good agreement in the scaling sense, meaning that all parameters differ by some coefficient that is approximately constant along the parts of the separator where reconnection is strongest. While the scaling is strong for all simulations, a comparison of absolute quantities shows that the quantitative agreement becomes progressively worse as the clock angle decreases.

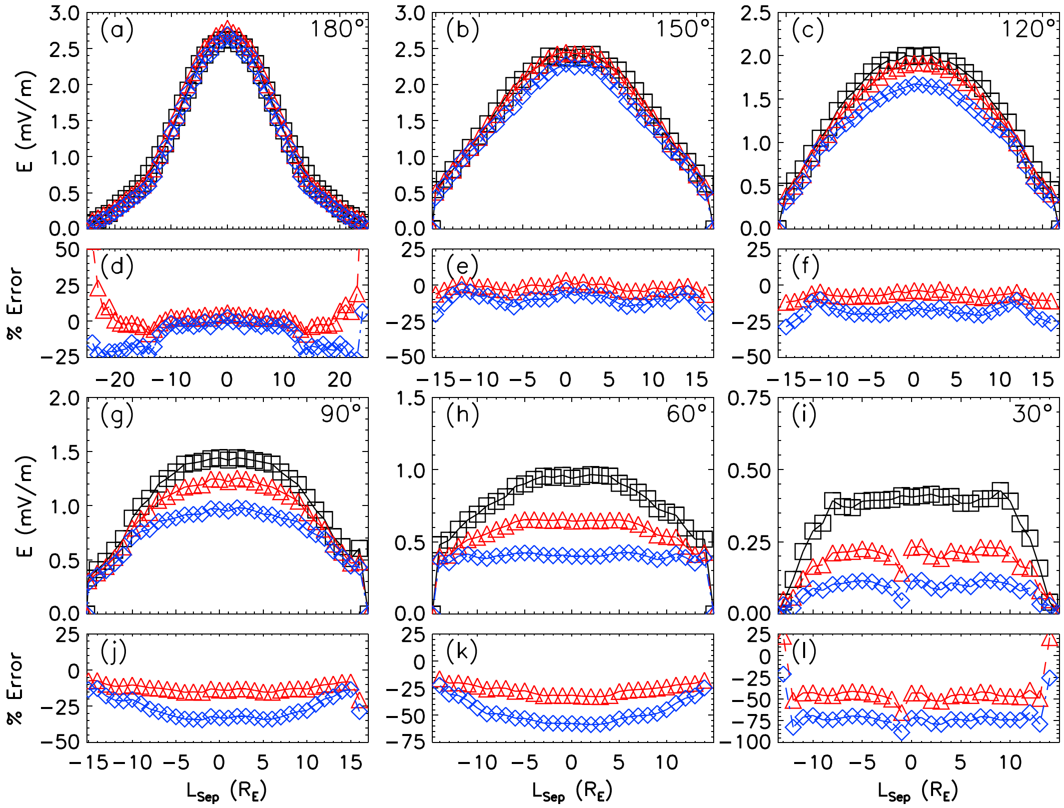

Figure 6. Comparison of the measured reconnection rate $E_{z'}$ (black □) at the X line with the theoretical E_{asym} (blue ◇) and the Sweet-Parker $E_{\eta,\mathrm{asym}}$ (red △) reconnection rates in distinct simulations with θ_{IMF} of (a) 180°, (b) 150°, (c) 120°, (g) 90°, (h) 60°, and (i) 30°. Percent errors between $E_{z'}$ and E_{asym} (blue ◇) or $E_{\eta,\mathrm{asym}}$ (red △) are displayed in Figures 6d–6f and 6j–6l. Electric fields are given in mV/m and all parameters are plotted as function of L_{Sep}, the duskward distance in R_E along the separator from the subsolar magnetopause.

As a way of quantifying the discrepancy between the measured reconnection rate and the predictions, the percent error between the measured reconnection rate $E_{z'}$ and the generalized asymmetric reconnection rate E_{asym} is calculated as a function of the distance along the separator as

$$\%\ \mathrm{Error} = \frac{E_{\mathrm{asym}} - E_{z'}}{E_{z'}} \times 100, \tag{10}$$

and for the asymmetric Sweet-Parker reconnection rate $E_{\eta,\mathrm{asym}}$ as

$$(\%\ \mathrm{Error})_{\eta} = \frac{E_{\eta,\mathrm{asym}} - E_{z'}}{E_{z'}} \times 100. \tag{11}$$

The percent errors from equation (10) for simulations with θ_{IMF} of (d) 180°, (e) 150°, (f) 120°, (j) 90°, (k) 60°, and (l) 30° are displayed as blue diamonds; those from equation (11) are red triangles. We note that through the subsolar magnetopause region ($|L_{\mathrm{Sep}}| \leq 5\ R_E$), E is significantly different from zero, and the percent error is relatively constant with distance along the X line. This implies the agreement is good in the scaling sense.

However, there is a trend that the percent error gets larger for smaller θ_{IMF} for both comparisons. The percent errors at the subsolar point for all simulations are given in Table 1. The dependence is described fairly well as the percent error being proportional to $-\cos\theta_{\mathrm{IMF}}$ (not shown). This suggests that there is a systematic effect causing an offset that increases with decreasing θ_{IMF}. One possible explanation is it could simply be a systematic effect in our algorithm to find δ or L or that the plane of reconnection is not normal to the X line for oblique IMF. It could also be physical, such as being related to the underlying assumption of the applicability of the 2-D asymmetric reconnection theory to the magnetopause.

Table 1. Percent Differences Between the Measured and Predicted Values of the Reconnection Rate $E_{z'}$ at the Subsolar Point

	180°	150°	120°	90°	60°	30°	120°, ψ=15°
%Error	2.67	−3.54	−15.79	−32.99	−57.62	−72.15	−20.80
$(\%\text{Error})_\eta$	5.92	3.44	−3.69	−13.79	−31.56	−43.00	−6.45
Prediction error	−3.07	−6.75	−12.56	−22.26	−38.07	−51.14	−15.34

We note that the two curves for $E_{\eta,\text{asym}}$ and E_{asym} should ideally lie on top of each other. However, in these cases there is some offset between the two. The error between the two predictions at the subsolar point is calculated using a form similar to equation (10) and substituting $E_{\eta,\text{asym}}$ for $E_{z'}$, and is given in the last row of Table 1. The results underscore that the differences may be attributed to the algorithm used to measure plasma parameters.

The simulations employed so far all have significant symmetry, so it is important to do similar comparisons for systems without symmetry. We therefore include a positive dipole tilt $\psi = 15°$ (northern geomagnetic pole oriented sunward) to break this symmetry. We use $\theta_{\text{IMF}} = 120°$ and all solar wind parameters the same as the previous simulations as a test case. Figure 7 displays the reconnection rate comparison as before for the dipole tilt simulation. We again see very good agreement in the scaling sense for both theoretical reconnection rates. The percent differences are calculated at the subsolar magnetopause as before, and we find the errors in E_{asym} and $E_{\eta,\text{asym}}$ to be −21% and −6.5%, respectively; these percent differences are comparable to those of the simulation with the same IMF clock angle but without any dipole tilt (see Table 1). This suggests that the prediction is equally successful with a dipole tilt.

Finally, we discuss an important aspect of an additional parametric test of the theory that could be the cause of confusion in future studies. We test smaller IMF strengths of 5 and 2 nT (from 20 nT). Each simulation uses $\theta_{\text{IMF}} = 120°$ without a dipole tilt and keeping all other solar wind parameters unchanged. From looking at the raw data, it appears that the agreement for the prediction compared to the measurement is much worse. The 5 nT simulation shows limited scaling agreement, and the 2 nT simulation does not reveal agreement even in the scaling sense.

It is important to realize, however, that the disagreement in this case is likely numerical. For smaller IMF strength, the magnetosheath reconnecting field strength decreases, leading to a larger asymmetry in magnetic field across the reconnection site. The larger the asymmetry, the more the X line and stagnation point are separated [*Cassak and Shay*, 2007]. As discussed in *Cassak and Shay* [2008], when the X line or stagnation

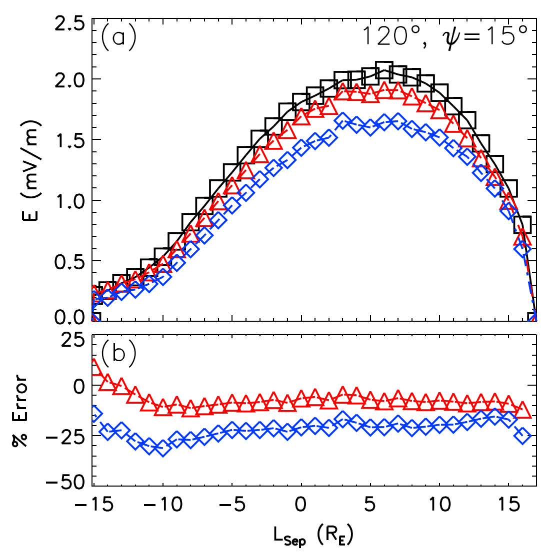

Figure 7. Comparison between the measured reconnection rate at the separator with the theoretical asymmetric reconnection rates in a simulation with θ_{IMF}=120° and positive dipole tilt of ψ=15°. See caption of Figure 6 for definitions.

point becomes less than a grid cell from the edge of the diffusion region, numerical problems arise. In these two simulations, the ratios of the magnetospheric reconnecting magnetic field component to the magnetosheath's are 0.2 and 0.1 for the $B_{\rm IMF} = 5$ and 2 nT simulations, respectively. The X line is located much closer to the edge of the magnetosheath current layer, and the distance between the two falls below our minimum simulation resolution of 0.125 R_E. Thus, the reconnection dynamics in the dissipation region are not sufficiently resolved. One would need maximum resolutions of 1/16 and 1/32 R_E in our $B_{\rm IMF} = 5$ and 2 nT simulations, respectively, to properly resolve the reconnection region substructure. Care should be taken on this issue in future studies.

4. Summary

In this study, we have investigated the local properties of magnetic reconnection at the dayside magnetopause in global MHD simulations. Previous studies have tested local reconnection theory in observations and simulations of reconnection at the dayside magnetopause for predominantly southward IMF, while the present work systematically finds the 3-D extent where reconnection is possible and tests the 2-D theory with oblique IMF and dipole tilt conditions.

The analysis presented here suggests that up to a scaling factor, the 2-D asymmetric reconnection theory accurately predicts the local reconnection rate at the dayside magnetopause as a function of the upstream parameters local to the magnetic X line for due southward IMF and without a dipole tilt. In simulations with oblique IMF, the analysis techniques are consistent with the scaling of the reconnection rate from 2-D asymmetric reconnection theory, up to an unspecified constant. The theory had been confirmed in previous global MHD simulations at the subsolar magnetopause for due southward IMF [*Borovsky et al.*, 2008; *Ouellette et al.*, 2014]. However, to the best of our knowledge, the present study is the first of its kind to analyze reconnection local to the X line for oblique IMF orientations and including a dipole tilt.

Interestingly, we have found an undetermined constant of proportionality between the scaling prediction from *Cassak and Shay* [2007] and the reconnection rates measured for oblique IMF, with the offset becoming more pronounced for smaller IMF clock angles. The cause of the offset is not understood, but it could either be a systematic effect based on how we determine the upstream parameters or a systematic limitation of applying the 2-D theory to the magnetosphere. Future work should be done to make this determination.

This study can be useful to help bridge the gap between reconnection physics local to the X line and how the magnetosphere globally reacts to given input from the solar wind. This is a core issue in the recent questions about whether local or global physics control dayside reconnection. Specifically, these techniques could be used to understand how plasmaspheric drainage plumes affect the local and global reconnection rates at the dayside magnetopause for arbitrary IMF and magnetospheric dipole tilt. However, this is beyond the scope of the present study and will be important for future work. It is hoped that similar tests can be performed with NASA's recently launched Magnetospheric Multiscale (MMS) mission [*Burch et al.*, 2015], which carries instruments with sufficient temporal and spatial resolution to observe reconnection and has spent a significant amount of time at the dayside magnetopause.

The approach used here to measure upstream plasma parameters locally at the X line should be useful in related work. There has been an increase in use of the Hall term in global magnetospheric simulations. The Hall effect was recently shown to significantly alter the global dynamics at Jupiter's moon Ganymede, with effects not seen in resistive MHD [*Dorelli et al.*, 2015]. The inclusion of the Hall term has profound implications on the local rate of reconnection, with Hall reconnection being much faster than collisional reconnection [*Birn et al.*, 2001]. Separators in the Ganymede Hall-MHD simulations were identified, but they were not used to calculate the local reconnection rate. This is because the parallel reconnection electric field from the Hall term vanishes since $\mathbf{E} \propto \mathbf{J}\times\mathbf{B}$. The fact that there is good agreement between the reconnection rate calculated from the parallel electric field, and the prediction based on upstream plasma parameters in the present study suggest that one can estimate the reconnection rate in Hall-MHD simulations by measuring the upstream plasma parameters and calculating the generalized reconnection rate $E_{\rm asym}$.

The present study employed a few underlying assumptions. For the global magnetospheric simulations, we employ a uniform, explicit resistivity even though Earth's magnetopause is essentially collisionless; this choice ensures our simulations are well resolved while reducing the likelihood of flux transfer events (FTEs)

[*Russell and Elphic*, 1978]. However, recent advances have been made to trace magnetic separators in simulations with FTEs [*Glocer et al.*, 2016], so this restriction is not required.

The present study does not take into account the effect of flow shear at the magnetopause due to the solar wind in equation (1) even though the theory of asymmetric reconnection with flow shear was recently worked out [*Doss et al.*, 2015]. However, the result of that study is that the flow shear becomes less important as the magnetosphere/magnetosheath asymmetries become more significant, so it is possible that the effect of the flow shear is not very large. Future work on this is required.

This study also does not take into account that the reconnection parameters are asymmetric in the outflow direction. This is especially true for essentially locations along the X line where symmetry is broken: locations away from the subsolar point for all but due southward IMF and no dipole tilt and everywhere when a dipole tilt is present. There are very few studies of this effect [*Murphy et al.*, 2010]. This effect undoubtedly is important and should be taken into account.

Further, the research detailed here uses idealized solar wind conditions with a few limitations not wholly representative of solar wind observations. The present work does not use an IMF B_x component, although it is expected that it affects reconnection in a similar way to systems with a dipole tilt. Previous studies found that under southward IMF orientations, the reconnection site moves northward for $B_x > 0$ and southward when $B_x < 0$ [*Peng et al.*, 2010; *Hoilijoki et al.*, 2014]. Additionally, our analysis is performed after the simulations have achieved a quasi-steady state, which does not capture the magnetosphere's response to dynamic solar wind conditions [*Laitinen et al.*, 2006, 2007]. Understanding the response of Earth's magnetosphere for a broader range of solar wind conditions is of the utmost importance for realistic space weather forecasting and will be the subject of future work.

Finally, this analysis is limited to the dayside portion of the X lines. The X line extends to the magnetotail where it forms a closed loop [*Laitinen et al.*, 2006, 2007]. The methodology here should work for locations extending further poleward of the magnetic nulls, like those found for northward IMF conditions described in *Komar et al.* [2015], but further research is necessary.

Acknowledgments
Support from NSF grant AGS-0953463 and NASA grant NNX10AN08A (PAC), and NASA West Virginia Space Grant Consortium (CMK) are gratefully acknowledged. Simulations were performed at the Community Coordinated Modeling Center at Goddard Space Flight Center through their public Runs on Request system (http://ccmc.gsfc.nasa.gov). The CCMC is a multi-agency partnership between NASA, AFMC, AFOSR, AFRL, AFWA, NOAA, NSF, and ONR. The BATS-R-US Model was developed by the Center for Space Environment Modeling at the University of Michigan. The analysis presented here was made possible via the Kameleon software package provided by the Community Coordinated Modeling Center at NASA Goddard Space Flight Center (http://ccmc.gsfc.nasa.gov). Software Developers are M.M. Maddox, D.H. Berrios, and L. Rastaetter. The data used to produce the results of this paper are publicly available for free from CCMC. The authors would like to thank J.C. Dorelli, B. Lavraud, Y.H. Liu, D.G. Sibeck, and F.D. Wilder for their insight and interesting discussions, and CMK thanks A. Glocer for his mentorship.

References

Axford, W. I. (1984), Magnetic field reconnection, in *Magnetic Reconnection in Space and Laboratory Plasmas*, edited by E. W. Hones, chap. 1, pp. 1–8, AGU, Washington, D. C., doi:10.1029/GM030p0001.

Beidler, M. T., and P. A. Cassak (2011), Model for incomplete reconnection in sawtooth crashes, *Phys. Rev. Lett.*, *107*, 255002, doi:10.1103/PhysRevLett.107.255002.

Beveridge, C. (2006), A new method for finding topological separators in a magnetic field, *Sol. Phys.*, *236*, 41–57, doi:10.1007/s11207-006-0124-3.

Birn, J., et al. (2001), Geospace Environmental Modeling (GEM) Magnetic Reconnection Challenge, *J. Geophys. Res.*, *106*, 3715–3719.

Birn, J., J. E. Borovsky, and M. Hesse (2008), Properties of asymmetric magnetic reconnection, *Phys. Plasmas*, *15*(3), 032101, doi:10.1063/1.2888491.

Borovsky, J. E., and M. H. Denton (2006), Effect of plasmaspheric drainage plumes on solar-wind/magnetosphere coupling, *Geophys. Res. Lett.*, *33*, L20101, doi:10.1029/2006GL026519.

Borovsky, J. E., and M. Hesse (2007), The reconnection of magnetic fields between plasmas with different densities: Scaling relations, *Phys. Plasmas*, *14*(10), 102309, doi:10.1063/1.2772619.

Borovsky, J. E., M. Hesse, J. Birn, and M. M. Kuznetsova (2008), What determines the reconnection rate at the dayside magnetosphere?, *J. Geophys. Res.*, *113*, A07210, doi:10.1029/2007JA012645.

Boudouridis, A., E. Zesta, L. R. Lyons, P. C. Anderson, and D. Lummerzheim (2005), Enhanced solar wind geoeffectiveness after a sudden increase in dynamic pressure during southward IMF orientation, *J. Geophys. Res.*, *110*, A05214, doi:10.1029/2004JA010704.

Burch, J. L., T. E. Moore, R. B. Torbert, and B. L. Giles (2015), Magnetospheric Multiscale overview and science objectives, *Space Sci. Rev.*, *199*(1), 5–21, doi:10.1007/s11214-015-0164-9.

Cassak, P. A., and M. A. Shay (2007), Scaling of asymmetric magnetic reconnection: General theory and collisional simulations, *Phys. Plasmas*, *14*, 102114.

Cassak, P. A., and M. A. Shay (2008), Scaling of asymmetric Hall magnetic reconnection, *Geophys. Res. Lett.*, *35*, L19102, doi:10.1029/2008GL035268.

Cassak, P. A., and M. A. Shay (2009), Structure of the dissipation region in fluid simulations of asymmetric magnetic reconnection, *Phys. Plasmas*, *16*, 055704.

Close, R. M., C. E. Parnell, and E. R. Priest (2004), Separators in 3D quiet-Sun magnetic fields, *Sol. Phys.*, *225*, 21–46.

De Zeeuw, D., T. Gombosi, C. Groth, K. Powell, and Q. Stout (2000), An adaptive MHD method for global space weather simulations, *IEEE Trans. Plasma Sci.*, *28*, 1956–1965.

Dorelli, J. C., A. Glocer, G. Collinson, and G. Tóth (2015), The role of the Hall effect in the global structure and dynamics of planetary magnetospheres: Ganymede as a case study, *J. Geophys. Res. Space Physics*, *120*, 5377–5392, doi:10.1002/2014JA020951.

Doss, C. E., C. M. Komar, P. A. Cassak, F. D. Wilder, S. Eriksson, and J. F. Drake (2015), Asymmetric magnetic reconnection with a flow shear and applications to the magnetopause, *J. Geophys. Res. Space Physics*, *120*, 7748–7763, doi:10.1002/2015JA021489.

Dungey, J. W. (1961), Interplanetary magnetic field and the auroral zones, *Phys. Rev. Lett.*, *6*, 47–48.

Dungey, J. W. (1963), The structure of the exosphere, or adventures in velocity space, in *Geophysics: The Earth's Environment*, edited by C. De Witt, J. Hieblot, and A. Lebeau, pp. 505–550, Gordon Breach, New York.
Glocer, A., J. Dorelli, G. Tóth, C. M. Komar, and P. A. Cassak (2016), Separator reconnection at the magnetopause for predominantly northward and southward IMF: Techniques and results, *J. Geophys. Res. Space Physics*, *121*, 140–156, doi:10.1002/2015JA021417.
Gombosi, T., D. DeZeeuw, C. Groth, and K. Powell (2000), Magnetospheric configuration for Parker-spiral IMF conditions: Results of a 3D AMR MHD simulation, *Adv. Space Res.*, *26*, 139–149.
Graham, D. B., Y. V. Khotyaintsev, A. Vaivads, M. André, and A. N. Fazakerley (2014), Electron dynamics in the diffusion region of an asymmetric magnetic reconnection, *Phys. Rev. Lett.*, *112*, 215004, doi:10.1103/PhysRevLett.112.215004.
Hesse, M., N. Aunai, S. Zenitani, M. Kuznetsova, and J. Birn (2013), Aspects of collisionless magnetic reconnection in asymmetric systems, *Phys. Plasmas*, *20*(6), 061210, doi:10.1063/1.4811467.
Hoilijoki, S., V. M. Souza, B. M. Walsh, P. Janhunen, and M. Palmroth (2014), Magnetopause reconnection and energy conversion as influenced by the dipole tilt and the IMF B_x, *J. Geophys. Res. Space Physics*, *119*, 4484–4494, doi:10.1002/2013JA019693.
Hu, Y. Q., X. C. Guo, and C. Wang (2007), On the ionospheric and reconnection potentials of the Earth: Results from global MHD simulations, *J. Geophys. Res.*, *112*, A07215, doi:10.1029/2006JA012145.
Komar, C. M., P. A. Cassak, J. C. Dorelli, A. Glocer, and M. M. Kuznetsova (2013), Tracing magnetic separators and their dependence on IMF clock angle in global magnetospheric simulations, *J. Geophys. Res. Space Physics*, *118*, 4998–5007, doi:10.1002/jgra.50479.
Komar, C. M., R. L. Fermo, and P. A. Cassak (2015), Comparative analysis of dayside magnetic reconnection models in global magnetosphere simulations, *J. Geophys. Res. Space Physics*, *120*, 276–294, doi:10.1002/2014JA020587.
Laitinen, T. V., P. Janhunen, T. I. Pulkkinen, M. Palmroth, and H. E. J. Koskinen (2006), On the characterization of magnetic reconnection in global MHD simulations, *Ann. Geophys.*, *24*, 3059–3069.
Laitinen, T. V., M. Palmroth, T. I. Pulkkinen, P. Janhunen, and H. E. J. Koskinen (2007), Continuous reconnection line and pressure-dependent energy conversion on the magnetopause in a global MHD model, *J. Geophys. Res.*, *112*, A11201, doi:10.1029/2007JA012352.
Longcope, D. W. (1996), Topology and current ribbons: A model for current, reconnection and flaring in a complex, evolving corona, *Sol. Phys.*, *169*, 91–121.
Lopez, R. E. (2016), The integrated dayside merging rate is controlled primarily by the solar wind, *J. Geophys. Res. Space Physics*, *121*, doi:10.1002/2016JA022556.
Malakit, K., M. A. Shay, P. A. Cassak, and C. Bard (2010), Scaling of asymmetric magnetic reconnection: Kinetic particle-in-cell simulations, *J. Geophys. Res.*, *115*, A10223, doi:10.1029/2010JA015452.
Malakit, K., M. A. Shay, P. A. Cassak, and D. Ruffolo (2013), New electric field in asymmetric magnetic reconnection, *Phys. Rev. Lett.*, *111*, 135001, doi:10.1103/PhysRevLett.111.135001.
Mozer, F. S., and A. Hull (2010), Scaling the energy conversion rate from magnetic field reconnection to different bodies, *Phys. Plasmas*, *17*(10), 102906, doi:10.1063/1.3504224.
Mozer, F. S., S. D. Bale, and T. D. Phan (2002), Evidence of diffusion regions at a subsolar magnetopause crossing, *Phys. Rev. Lett.*, *89*, 015002, doi:10.1103/PhysRevLett.89.015002.
Murphy, N. A., C. R. Sovinec, and P. A. Cassak (2010), Magnetic reconnection with asymmetry in the outflow direction, *J. Geophys. Res.*, *115*, A09206, doi:10.1029/2009JA015183.
Murphy, N. A., M. P. Miralles, C. L. Pope, J. C. Raymond, H. D. Winter, K. K. Reeves, D. B. Seaton, A. A. van Ballegooijen, and J. Lin (2012), Asymmetric magnetic reconnection in solar flare and coronal mass ejection current sheets, *Astrophys. J.*, *751*(1), 56.
Muzamil, F. M., C. J. Farrugia, R. B. Torbert, P. R. Pritchett, F. S. Mozer, J. D. Scudder, C. T. Russell, P. E. Sandholt, W. F. Denig, and L. Wilson (2014), Structure of a reconnection layer poleward of the cusp: Extreme density asymmetry and a guide field, *J. Geophys. Res. Space Physics*, *119*, 7343–7362, doi:10.1002/2014JA019879.
Newell, P. T., T. Sotirelis, K. Liou, C.-I. Meng, and F. J. Rich (2007), A nearly universal solar wind-magnetosphere coupling function inferred from 10 magnetospheric state variables, *J. Geophys. Res.*, *112*, A01206, doi:10.1029/2006JA012015.
Ouellette, J. E., J. G. Lyon, and B. N. Rogers (2014), A study of asymmetric reconnection scaling in the Lyon-Fedder-Mobarry code, *J. Geophys. Res. Space Physics*, *119*, 1673–1682, doi:10.1002/2013JA019366.
Ouellette, J. E., J. G. Lyon, O. J. Brambles, B. Zhang, and W. Lotko (2016), The effects of plasmaspheric plumes on dayside reconnection, *J. Geophys. Res. Space Physics*, *121*, doi:10.1002/2016JA022597.
Parker, E. N. (1957), Sweet's mechanism for merging magnetic fields in conducting fluids, *J. Geophys. Res.*, *62*, 509–520.
Parnell, C. E., A. L. Haynes, and K. Galsgaard (2010), Structure of magnetic separators and separator reconnection, *J. Geophys. Res.*, *115*, A02102, doi:10.1029/2009JA014557.
Peng, Z., C. Wang, and Y. Q. Hu (2010), Role of IMF B_x in the solar wind-magnetosphere-ionosphere coupling, *J. Geophys. Res.*, *115*, A08224, doi:10.1029/2010JA015454.
Powell, K. G., P. L. Roe, T. J. Linde, T. I. Gombosi, and D. L. D. Zeeuw (1999), A solution-adaptive upwind scheme for ideal magnetohydrodynamics, *J. Comput. Phys.*, *154*, 284–309.
Pu, Z. Y., J. Raeder, J. Zhong, Y. V. Bogdanova, M. Dunlop, C. J. Xiao, X. G. Wang, and A. Fazakerley (2013), Magnetic topologies of an in vivo FTE observed by Double Star/TC-1 at Earth's magnetopause, *Geophys. Res. Lett.*, *40*, 3502–3506, doi:10.1002/grl.50714.
Rosenberg, M. J., C. K. Li, W. Fox, I. Igumenshchev, F. H. Séguin, R. P. J. Town, J. A. Frenje, C. Stoeckl, V. Glebov, and R. D. Petrasso (2015), A laboratory study of asymmetric magnetic reconnection in strongly driven plasmas, *Nat. Commun.*, *6*, 6190.
Russell, C. T., and R. C. Elphic (1978), Initial ISEE magnetometer results: Magnetopause observations, *Space Sci. Rev.*, *22*, 681–715.
Sandel, B., J. Goldstein, D. Gallagher, and M. Spasojevic (2003), Extreme ultraviolet imager observations of the structure and dynamics of the plasmasphere, *Space Sci. Rev.*, *109*(1–4), 25–46, doi:10.1023/B:SPAC.0000007511.47727.5b.
Servidio, S., W. H. Matthaeus, M. A. Shay, P. A. Cassak, and P. Dmitruk (2009), Magnetic reconnection in two-dimensional magnetohydrodynamic turbulence, *Phys. Rev. Lett.*, *102*, 115003, doi:10.1103/PhysRevLett.102.115003.
Sonnerup, B. U. Ö., and L. J. Cahill (1967), Magnetopause structure and attitude from Explorer 12 observations, *J. Geophys. Res.*, *72*(1), 171–183, doi:10.1029/JZ072i001p00171.
Stevenson, J. E. H., and C. E. Parnell (2015), Spontaneous reconnection at a separator current layer: 1. Nature of the reconnection, *J. Geophys. Res. Space Physics*, *120*, 10,334–10,352, doi:10.1002/2015JA021730.
Sweet, P. A. (1958), The neutral point theory of solar flares, in *Electromagnetic Phenomena in Cosmical Physics, IAU Symposium*, vol. 6, edited by B. Lehnert, pp. 123–134, Cambridge Univ. Press, Cambridge, U. K.
Swisdak, M., and J. F. Drake (2007), Orientation of the reconnection X-line, *Geophys. Res. Lett.*, *34*, L11106, doi:10.1029/2007GL029815.
Swisdak, M., J. F. Drake, M. A. Shay, and B. N. Rogers (2003), Diamagnetic suppression of component magnetic reconnection at the magnetopause, *J. Geophys. Res.*, *108*(A5), 1218, doi:10.1029/2002JA009726.

Swisdak, M., M. Opher, J. F. Drake, and F. A. Bibi (2010), The vector direction of the interstellar magnetic field outside the heliosphere, *Astrophys. J.*, *710*(2), 1769–1775.
Tóth, G., et al. (2005), Space Weather Modeling Framework: A new tool for the space science community, *J. Geophys. Res.*, *110*, A12226, doi:10.1029/2005JA011126.
Tóth, G., et al. (2012), Adaptive numerical algorithms in space weather modeling, *J. Comput. Phys.*, *231*(3), 870–903, doi:10.1016/j.jcp.2011.02.006.
Trattner, K. J., J. S. Mulcock, S. M. Petrinec, and S. A. Fuselier (2007), Probing the boundary between antiparallel and component reconnection during southward interplanetary magnetic field conditions, *J. Geophys. Res.*, *112*, A08210, doi:10.1029/2007JA012270.
Walsh, B. M., J. C. Foster, P. J. Erickson, and D. G. Sibeck (2014a), Simultaneous ground- and space-based observations of the plasmaspheric plume and reconnection, *Science*, *343*(6175), 1122–1125, doi:10.1126/science.1247212.
Walsh, B. M., T. D. Phan, D. G. Sibeck, and V. M. Souza (2014b), The plasmaspheric plume and magnetopause reconnection, *Geophys. Res. Lett.*, *41*, 223–228, doi:10.1002/2013GL058802.
Wang, S., L. M. Kistler, C. G. Mouikis, and S. M. Petrinec (2015), Dependence of the dayside magnetopause reconnection rate on local conditions, *J. Geophys. Res. Space Physics*, *120*, 6386–6408, doi:10.1002/2015JA021524.
Xiao, C. J., et al. (2007), Satellite observations of separator-line geometry of three-dimensional magnetic reconnection, *Nat. Phys.*, *3*, 609–613.
Yoo, J., M. Yamada, H. Ji, J. Jara-Almonte, C. E. Myers, and L.-J. Chen (2014), Laboratory study of magnetic reconnection with a density asymmetry across the current sheet, *Phys. Rev. Lett.*, *113*, 095002, doi:10.1103/PhysRevLett.113.095002.
Zhang, B., O. J. Brambles, M. Wiltberger, W. Lotko, J. E. Ouellette, and J. G. Lyon (2016), How does mass loading impact local versus global control on dayside reconnection?, *Geophys. Res. Lett.*, *43*, 1837–1844, doi:10.1002/2016GL068005.